PHYSICAL REVIEW D, VOLUME 64, 054004

# Phenomenological approach of multiple particle production at high energies: Energy distribution of produced particles by data of direct observation

Akinori Ohsawa
*Institute for Cosmic Ray Research, University of Tokyo, Kashiwa, Chiba, 277-8582 Japan*

Edison H. Shibuya
*Instituto de Fisica Gleb Wataghin, Universidade Estadual de Campinas, 13083-970 Campinas, São Paulo, Brasil*

Masanobu Tamada
*Faculty of Science and Technology, Kinki University, Higashi-Osaka, Osaka, 577-8502 Japan*

(Received 11 November 2000; published 6 August 2001)

The energy distribution of produced particles in *multiple particle production* is formulated empirically based on the data of direct observations by accelerator and cosmic-ray experiments at $10^{12}$–$10^{14}$ eV. The formulated distribution indicates violation of the Feynman scaling law, which was shown to be valid in the low energy region of $\leqslant 10^{12}$ eV. That is, the particle density is suppressed in the forward region and enhanced in the central region, compared with the distribution of the Feynman scaling law. The consequences of the formulated distribution, such as multiplicity, inelasticity, etc., are discussed at high energies of $\geqslant 10^{15}$ eV by extrapolation. The distribution is also compared with those of nuclear interaction models which are used widely in simulations of accelerator and cosmic-ray experiments.

DOI: 10.1103/PhysRevD.64.054004 PACS number(s): 13.85.Hd, 13.85.Tp

## I. INTRODUCTION

The study of multiple particle production (MPP) is important for particle physics, because it may offer useful information to perturbative and nonperturbative quantum chromodynamics, the mechanism of the color confinement and formation of strings.

The study is important for high energy cosmic-ray physics, too, because MPP is one of the main processes which govern high energy cosmic-ray diffusion in the atmosphere. Experimental data of high energy cosmic-ray phenomena, much of which are obtained by ground-based experiment, are analyzed usually by assuming a certain model of MPP. Consequently many of the conclusions which are obtained by analyzing high energy cosmic-ray phenomena are model-dependent ones, with each different model predicting a different feature of MPP.

There are various models, theoretical and phenomenological, to describe MPP. However these models do not predict the features of MPP consistently with each other, and do not succeed in describing the existing experimental data in a satisfactory manner. A discrepancy between the model predictions and experimental data is discussed in this paper for the data of direct observations at $10^{14}$ eV. There are several indications that experimental data of cosmic rays are not described well by the current models in the primary energy region exceeding $\sim 10^{15}$ eV [1].

To discuss MPP, it is convenient to start from the energy distribution of produced particles, since some important features of MPP, such as inelasticity and multiplicity, are derived from it. To discuss the energy distribution, however, we have almost no *a priori* guiding principles except energy conservation. On the other hand a theoretical approach cannot yet describe MPP without ambiguity. Furthermore, there are many theoretical models to address different features of MPP, as mentioned above.

In given present circumstances, it may be reasonable to take a phenomenological approach or to start from experimental data while as much as possible trying to avoid assumptions without experimental basis. It is pertinent to discuss MPP models now, because available data exists in a wide energy region, i.e., accelerator data at $10^{14}$ eV, data from mountain emulsion chamber experiments at $\sim 10^{15}$ eV, data from air shower experiments at $\sim 10^{16}$ eV, and data of highest energy air showers at $\geqslant 10^{18}$ eV.

As the first step we examine the data from direct observation by accelerator and cosmic-ray experiments in the energy region of $\sim 10^{14}$ eV, and formulate an energy distribution of produced particles based on the Feynman scaling law with scaling violation parameters.

Validity of the formulated model will be tested first of all in the highest energy regions of $\geqslant 10^{18}$ eV, which will be made in the succeeding papers. The advantage in examining the highest energy events is that the energy dependence of the formulated model appears in an easily distinguished way. In other words, the difference of respective models is not large in the energy region $10^{15}$–$10^{16}$ eV. If the formulated model fails to describe the highest energy events, we must find another formulation based on the data from cosmic-ray experiments at $10^{15}$–$10^{17}$ eV.

Our study is made in the following way. Assuming the energy distribution of produced particles, which tends to that of the Feynman scaling law at low energies, we determine magnitudes of the scaling violation parameters at various collision energies where the experimental data is available. Assuming that the obtained energy dependence of the scaling violation parameters is valid up to $10^{20}$ eV, we discuss the consequences of the formulated distribution at higher energies. The formulated distribution is compared with the predictions of models which are used widely in simulations in accelerator and cosmic-ray experiments.

 

TABLE I. List of the experiments and their respective measurements.

| Group | Site | Collision | Energy $\sqrt{s}$ (GeV) | Maximum rapidity | Presented quantity | Observed particles | Observed region |
|---|---|---|---|---|---|---|---|
| Brazil-Japan Collab. [6] | Mt. Chacaltaya | $h$-$C$[a] | 500[b] | $y_{max}=12.2$ | $dN/dy_{\gamma}$ | $\gamma$-rays | $y_{\gamma}\geqslant 7.8$ |
| | | | 53 | $y^*_{max}=4.0$ | $dN/d\eta^*$ | charged | |
| UA5 Collab. [7] | CERN | $\overline{p}p$ | 200 | $y^*_{max}=5.3$ | $dN/d\eta^*$ | charged | $\lvert\eta^*\rvert<4.5$ |
| | | | 546 | $y^*_{max}=6.3$ | $dN/d\eta^*$ | charged | |
| | | | 900 | $y^*_{max}=6.8$ | $dN/d\eta^*$ | charged | |
| UA7 Collab. [8] | CERN | $\overline{p}p$ | 630 | $y^*_{max}=6.4$ | $dN/dy^*$ | $\pi^0$ | $y^*=5.0\sim 6.6$ |
| Harr *et al.* [9] | CERN | $\overline{p}p$ | 630 | $y^*_{max}=6.4$ | $dN/d\eta^*$ | charged | $\eta^*=1.5\sim 5.5$ |

[a]Hadron (nucleon, pion)-carbon collisions.
[b]The value is the averaged one, i.e., $\langle\sqrt{s}\rangle=500$ GeV.

## II. ENERGY DISTRIBUTION OF PRODUCED PARTICLES

In this section we discuss the energy distribution of produced particles in $N$–$N$ (nucleon-nucleon) inelastic collisions under the assumption that the final state of multiple particle production consists of a surviving particle, which has the same particle nature as the incident particle, and the produced particles. The view is valid empirically if one assumes that the energy of the surviving particle is distributed between 0 and $E_0$ in the laboratory system.[1] Note that the surviving particle is not always the leading particle or the highest energy particle. Plausibility of the assumption was discussed in detail in Ref. [2]. This approach does not require specifying kinds of produced particles at all.

### A. Scaling function

Feynman assumed that the energy distribution of produced particles in multiple particle production, expressed by the variable $x^*\equiv 2p^*_{\|}/\sqrt{s}$ ($p^*_{\|}$: the longitudinal component of the momentum vector $\boldsymbol{p}^*$ of the produced particle),[2] is independent of the incident energy $\sqrt{s}$ at high energies [3]. This assumption appeared to be valid up to the energy of $\sqrt{s}=63$ GeV, the maximum available energy at that time [4]. One of the empirical formulas to express the energy distribution of *charged* produced particles is [5]

$$\frac{1}{\sigma_{inel}}\frac{d\sigma}{dx^*}\equiv\varphi_0(x^*)=D\frac{(1-x^*)^d}{x^*}, \qquad (1)$$

where

$$D=\frac{d+1}{3}=1.67, \quad d=4.0.$$

The distribution is called "the scaling function" hereafter, and matches the experimental data well as can be seen in Fig. 5.

As the relation $x^*\simeq E/E_0\equiv x$ is valid at high energy, Eq. (1) has an expression,

$$\varphi_0(x)dx\simeq D\frac{(1-x)^d}{x}dx \qquad (2)$$

in the laboratory system, and the average value of the total inelasticity[3] is

$$\langle K\rangle\equiv\frac{3}{2}\int_0^1 x\varphi_0(x)dx=0.5 \qquad (3)$$

where the factor 3/2 should be modified slightly when all the produced particles are not pions. The energy dependence of the charged particle multiplicity is given by

$$m(E_0)\equiv\int_{m_\pi/E_0}^1\varphi_0(x)dx\simeq D\left[\ln\left(\frac{E_0}{m_\pi}\right)-\frac{25}{12}\right] \qquad (4)$$

which matches the experimental data fairly well in the low energy region (see Fig. 6).

### B. $dN/dy^*$ and $dN/d\eta^*$ from $dN/dx^*$

At still higher energies, there are several data sets of direct observation by cosmic-ray and accelerator experiments, which are tabulated chronologically in Table I. Note that the experimental data are presented in various quantities, such as rapidity density, pseudo-rapidity density, etc., owing to the experimental conditions of the respective groups.

To compare the data in Table I with the scaling function, one has to transform $dN/dx^*$ into $dN/d\eta^*$, $dN/dy^*$, etc. In doing so, one has to take into account that the average value of the transverse momentum $\langle p_T\rangle$ depends on the rapidity, i.e., the value becomes smaller in the forward region [10].

[1]Strictly speaking, the energy of the surviving particle is assumed to be distributed between $E_1=\max(0,2\langle K\rangle-1)E_0$ and $E_2=\min(2\langle K\rangle,1)E_0$ in the laboratory system, depending on the average value of the inelasticity $\langle K\rangle$. That is, the energy is distributed between 0 and 1 when $\langle K\rangle=0.5$.

[2]The quantities with and without an asterisk (*) are those in the center of mass system and in the laboratory system, respectively.

[3]The energy distribution of produced particles $\varphi_0(x)dx$ is the averaged one with respect to the inelasticity distribution.

Following the analysis which was made by one of the present authors [11], we assume that $x$ distribution of the *charged* produced particles is expressed in the following way:

$$\frac{dN}{dx^* dp_T} = aD \frac{(1-a' x^*)^d}{\sqrt{x^{*2}+(2\mu/\sqrt{s})^2}} g(p_T) \quad \left(\mu \equiv \sqrt{p_T^2+m_\pi^2}\right), \tag{5}$$

where the parameters $a$ and $a'$ are adjustable. This formula reproduces the scaling function of Eq. (1) using $a=a'=1$ and $\sqrt{s}\to\infty$. The parameters $a$ $(\geqslant 1)$ and $a'$ $(\geqslant 1)$ express enhancement of the scaling function in the central region and suppression in the forward region, respectively.[4] The meaning of the term $2\mu/\sqrt{s}$ is discussed below.

The $p_T$ distribution is assumed to be

$$g(p_T)dp_T = p_T \exp\left(-\frac{p_T}{p_0}\right)\frac{dp_T}{p_0^2} \tag{6}$$

with

$$p_0 = \begin{cases} c & (x^* < x_0^*) \\ c\left(\dfrac{x_0^*}{x^*}\right)^{c'} & (x^* > x_0^*) \end{cases} \quad (c=0.2 \ \text{GeV}/c, \ c'=0.57, \ x_0^*=0.08). \tag{7}$$

According to the $p_T$ distribution of Eq.(6), the average value of $p_T$, $\langle p_T\rangle = 2p_0$, becomes smaller in the forward region $x^*>x_0^*$, which is observed by the experiments [10,8]. The values of $c'$ and $x_0^*$ are determined in Appendix A.

There are several points of improvement or modification from the previous work of Ref. [11], and they lead to a slightly different conclusion about the degree of scaling violation due to different $p_T$ dependence of the adopted function. These are

(1) The distribution is factorized into $dN/dx^*$ and $g(p_T)$ in this work, while into $dN/dy^*$ and $g(p_T)$ in the previous work. It is evident that present factorization is better, because $x^*$ is independent of $p_T$ but $y^*$ is not.

(2) The denominator of the distribution is $\sqrt{x^{*2}+(2\mu/\sqrt{s})^2}$ in this work but $x^*$ in the previous work. The present one is better because otherwise $dN/dy^*$ is divergent at $y^*=0$. (See the comment in Sec. II D, too.)

Since the definitions of the Feynman variable $(x^*)$, the rapidity $(y^*)$ and the pseudo-rapidity $(\eta^*)$ are

$$x^* \equiv \frac{2p_{\|}^*}{\sqrt{s}},$$

$$y^* \equiv \frac{1}{2}\ln\frac{E^*+p_{\|}^*}{E^*-p_{\|}^*} \quad \text{or} \quad x^* = \frac{\mu}{\sqrt{s}}(e^{y^*}-e^{-y^*}),$$

$$\eta^* \equiv \frac{1}{2}\ln\frac{p^*+p_{\|}^*}{p^*-p_{\|}^*} \quad \text{or} \quad x^* = \frac{p_T}{\sqrt{s}}(e^{\eta^*}-e^{-\eta^*}),$$

we have

$$\frac{dN}{dy^* dp_T} = \frac{dN}{dx^* dp_T}\frac{\partial x^*}{\partial y^*} = aD\left[1-a'\frac{\mu}{\sqrt{s}}(e^{y^*}-e^{-y^*})\right]^d g(p_T), \tag{8}$$

$$\frac{dN}{d\eta^* dp_T} = aD\left[1-a'\frac{p_T}{\sqrt{s}}(e^{\eta^*}-e^{-\eta^*})\right]^d \times \frac{(e^{\eta^*}+e^{-\eta^*})}{\sqrt{(e^{\eta^*}-e^{-\eta^*})^2+\left(\dfrac{2\mu}{p_T}\right)^2}} g(p_T). \tag{9}$$

The distributions $dN/dy^*$ and $dN/d\eta^*$ are obtained by numerical integration with respect to the transverse momentum $p_T$. The parameter $p_0$ in Eq. (7) is expressed by the rapidity $y^*$ and the pseudo-rapidity $\eta^*$ in the following way:

$$p_0 = \begin{cases} c & (y^* < y_0^*) \\ ce^{-c'(y^*-y_0^*)} & (y^* > y_0^*) \end{cases} \quad (y_0^* = y_c - 1.5) \tag{10}$$

and

$$p_0 = \begin{cases} c & (\eta^* < \eta_0^*) \\ ce^{-c'(\eta^*-\eta_0^*)} & (\eta^* > \eta_0^*) \end{cases} \quad (\eta_0^* = y_c - 1.3), \tag{11}$$

[4] Increase of the value $a$ also brings an increase in the distribution in the forward region. In this sense $a$ and $a'$ do not work "independently."

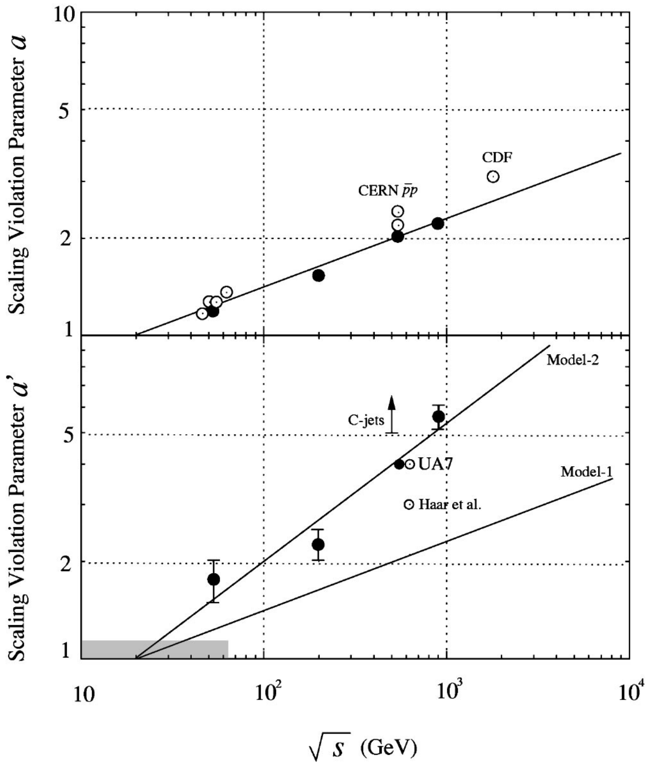


FIG. 1. Energy dependence of the scaling violation parameters, $a$ (the upper figure) and $a'$ (lower) in Eq. (5) in the text. Plots are obtained by fitting the calculated curves of (pseudo-)rapidity density distribution to those of the experimental data. The full circles are from the experimental data of the UA5 Collaboration [7], and the open circles are from those of other experimental groups [7,12,9]. All the experimental data are listed in Ref. [7]. The bar with an arrow, indicated as ''C-jets,'' is from the cosmic-ray experiment [6]. The hatched area indicates the energy region where the Feynman scaling law ($a \simeq 1.0$ and $a' \simeq 1.0$) is verified by the experiments. The lines are the assumed energy dependences in model 1 and model 2.

where $c' = 1/1.76 = 0.57$. Derivations of Eqs. (10) and (11) can be found in Appendix A. The distribution of $\gamma$ rays, which is to be used for analyzing Chacaltaya emulsion chamber data, is discussed in Appendix B.

### C. Scaling violation parameters

Using Eqs. (8) and (9), we can calculate the (pseudo-) rapidity density distribution at the incident energy $\sqrt{s}$ for various values of the parameters $a$ and $a'$, which are to be compared with those of the experimental data. We assume the energy dependence of parameter $a$ as

$$a = \left(\frac{s}{s_0}\right)^{\alpha} \simeq \left(\frac{E_0}{A}\right)^{\alpha} \quad (s = 2ME_0 + 2M^2 \simeq 2ME_0) \quad (12)$$

with

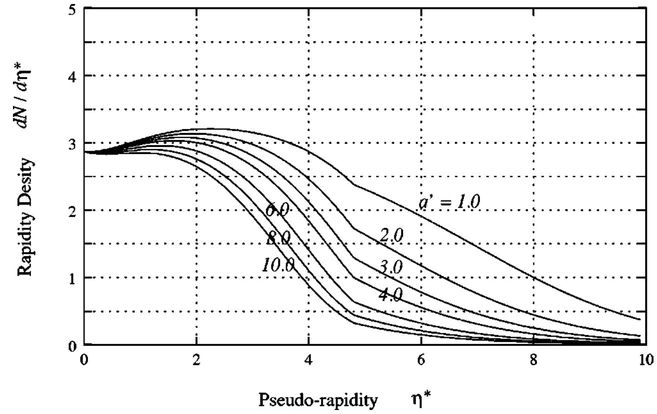


FIG. 2. Pseudo-rapidity density distributions at $\sqrt{s} = 546$ GeV for various values of the scaling violation parameter $a'$. The parameter $a$ is given by Eq. (12) in the text. The kink in the curve at $\eta^* = 4.8$ is due to the rapidity dependence of the average $p_T$ value.

$$s_0 = 3.9 \times 10^2 \ \text{GeV}^2, \quad A = \frac{s_0}{2M} = 2.0 \times 10^2 \ \text{GeV} \ \text{and}$$

$$\alpha = 0.105.$$

The energy dependence of the parameter $a$ is shown in Fig. 1 together with experimental data. Then the pseudorapidity density at $\eta^* = 0$ is given by

$$\left(\frac{dN}{d\eta^*}\right)_{\eta^*=0} = D\left\langle \frac{p_T}{\sqrt{p_T^2 + m_\pi^2}} \right\rangle a = 1.67 \times 0.83 \times \left(\frac{s}{s_0}\right)^{\alpha}, \quad (13)$$

which reproduces $\rho(0) = 0.74 s^{0.105}$ found by the UA5 Collaboration [7]. It may be worth mentioning that the data of $\rho(0)$, the pseudo-rapidity density at $\eta^* = 0$, is a reliable quantity in a collider-type accelerator experiment. Figure 2 shows the pseudo-rapidity distributions at $\sqrt{s} = 546$ GeV for various values of the scaling violation parameter $a'$.

The calculated distributions are compared with the experimental data, listed in Table I, with an aim at finding the value of the scaling violation parameter $a'$. In fitting the curves to the experimental data we put a heavier weight on the data points in the forward region than those in the plateau of the distribution because the density in the plateau is almost fixed by the parameter $a$. For example, in Fig. 3 the best-fit curve is consistent with the data points in the forward region in the case of $\sqrt{s} = 53$ GeV. The data are those of all inelastic events but not only NSD (nonsingle-diffractive) events,[5] be-

[5]Definitions of all inelastic events and NSD events are

$$\sigma_{inel} = \sigma_{NSD} + \sigma_{SD} \quad \text{and} \quad \sigma_{NSD} = \sigma_{ND} + \sigma_{DD}$$

where ND, SD, and DD stand for ''nondiffractive,'' ''single-diffractive'' and ''double-diffractive'' events. According to the UA5 Collaboration data, the density of the former is 10% smaller than that of the latter in the pseudo-rapidity range $0 \leqslant \eta^* \leqslant 3.5$ and is almost equal to that of the latter in $\eta^* \geqslant 3.5$ at $\sqrt{s} = 546$ GeV [7].

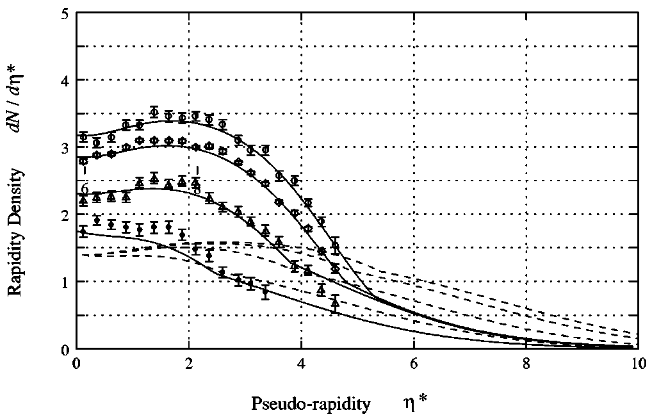


FIG. 3. Pseudo-rapidity density distributions by UA5 Collaboration experiment (plots), those of model 2 (solid lines), and those of model 0 (chain lines). The data are those of all inelastic events at the energies of $\sqrt{s}=53$ GeV (●), 200 GeV (△), 546 GeV (◇), and 900 GeV (○). The solid lines are by model 2 with the parameter values $a'$ of the best fitting at respective energies.

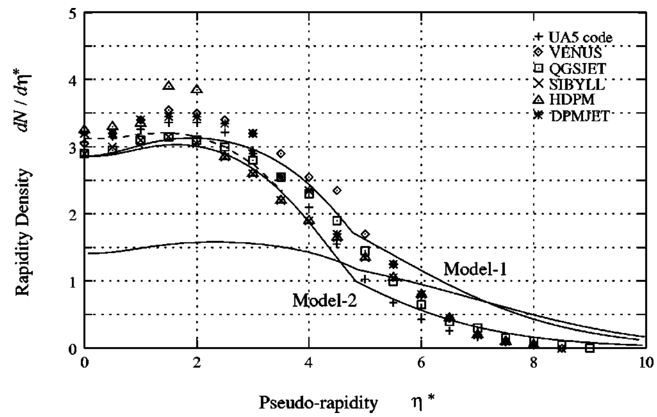


FIG. 4. Pseudo-rapidity density distributions at $\sqrt{s}=546$ GeV. Plots are by the simulation models (UA5 code, VENUS, QGSJET, SIBYLL, HDPM, and DPMJET). The data by the simulations are based on the NSD (nonsingle-diffractive) events, while those by model 0, model 1, and model 2 (solid lines) are for all inelastic events. See the footnote([5]) for the difference between NSD and all inelastic events. The chain line is that of model 2 which is corrected for NSD events following the comment in the footnote([5]).

cause the former is more suitable for discussing cosmic-ray diffusion. The energy dependence of the scaling violation parameters $a$ and $a'$ are shown in Fig. 1, where we observe that the parameter $a'$ has a stronger dependence than the parameter $a$.

From the energy dependence of the parameters $a$ and $a'$ in Fig. 1, we assume two cases of

$$a'=\left(\frac{E_0}{A}\right)^{\alpha'} \quad (\alpha'=0.105 \quad \text{and} \quad 0.210), \tag{14}$$

which are called model 1 and model 2 hereafter. The parameters $a$ and $a'$ in model 1 have the same energy dependence, and those in model 2 are the best fit to the experimental data. Note that the data from Harr *et al.* and from the C-jets of the Chacaltaya experiment deviate from the line of model 2. Model 0 with $a=a'=1.0$, which stands for the case of Feynman scaling law, is included for reference (Table II).

To show how the experimental data are described by the formula of Eq. (9) with appropriate values of the parameters $a$ and $a'$, Fig. 3 presents the pseudo-rapidity density distributions of all inelastic events (but not only of nonsingle-diffractive events) recorded by the UA5 Collaboration together with those of the formulated models. One can see in the figure that the reproduction is satisfactory by model 2 and that model 0 (the Feynman scaling law) cannot reproduce the data both in the central and forward regions. Note that the distribution of model 0 is slightly energy dependent, as can be seen in Eq. (5).

It is also interesting to see how the formulated distribution is reproduced by the models which are used recently in simulations of atmospheric cosmic-ray diffusion. In Fig. 4 we compare the pseudo-rapidity density distributions [13], predicted by UA5 code [14],[6] VENUS [15], QGSJET [16], SIBYLL [17], HDPM [18], and DPMJET [19] with those of the present models. The simulation models VENUS, QGSJET, and DPMJET are based on Gribov-Regge theory of soft hadronic collisions, while UA5 code, SIBYLL and HDPM are fully or partly phenomenological. Note that the pseudo-rapidity density by simulations is for NSD (nonsingle-diffractive) events while that of the calculation is for all inelastic events.

Table III presents the dispersions of the pseudo-rapidity distribution between model 2 and respective simulation models in Fig. 4. The dispersion $\sigma$ is defined as

$$\sigma=\sqrt{\frac{S}{n}} \quad \text{with} \quad S=\sum_{i=1}^{n}\left[\left(\frac{dN}{d\eta^*}\right)_{\text{sim}}-\left(\frac{dN}{d\eta^*}\right)_{\text{model 2}}\right]^2_{\eta^*=\eta_i^*}$$

where $n$ is the number of data points. In calculating the dispersions the rapidity density distribution of model 2 is corrected for NSD events, following comments in the footnote ([5]), which is also shown in Fig. 4. In the table we present three values of different rapidity range; $\eta^*=0\sim3.0$, $\eta^*=3.5\sim6.0$, and $\eta^*=6.5\sim8.0$. Note that $\eta^*=5.0$ corresponds to $x^*=0.1$ at $\sqrt{s}=546$ GeV. That is, the three ranges correspond roughly to the central, middle, and forward regions, respectively, among which the middle region is the most important for cosmic-ray diffusion in the atmosphere.

The following observations can be made from the table and Fig. 4.

(1) In the central region the distributions are similar except that of HDPM.

(2) In the middle region QGSJET, VENUS, DPMJET predict higher density appreciably than that of model 2.

[6]UA5 Collaboration made a simulation code which describes the data observed by the collaboration.

TABLE II. Scaling violation parameters, assumed in the models.

| Model | Scaling-violation parameters [a] $a=\left(\frac{E_0}{A}\right)^{\alpha}$ | $a'=\left(\frac{E_0}{A}\right)^{\alpha'}$ | Average inelasticity | Remarks |
|---|---|---|---|---|
| Model 0 | $\alpha=0$ | $\alpha'=0$ | $\langle K\rangle=0.5$ | the Feynman scaling law |
| Model 1 | $\alpha=0.105$ | $\alpha'=0.105$ | $\langle K\rangle=0.5$ | |
| Model 2 | $\alpha=0.105$ | $\alpha'=0.210$ | $\langle K\rangle=0.5(E_0/A)^{-0.105}$ | the best fit to the experimental data |

[a] $A=2.0\times10^2$ GeV.

(3) In the forward region all the model predictions are almost consistent.

(4) UA5 code predicts the most consistent distribution with that of model 2.[7] Figure 4 also suggests,

(5) The difference of the rapidity densities, predicted by respective simulation models, is not negligibly small.

(6) The experimental data of Harr *et al.* is almost consistent with those by QGSJET (see also the lower figure in Fig. 1).

(7) The rapidity density of the QGSJET model, which is used frequently at present in simulations of cosmic-ray phenomena, is almost between those of model 1 and model 2.

### D. *x* distribution, multiplicity and inelasticity, predicted by the models

Using an approximate relation $x^*\simeq E/E_0\equiv x$ valid at high energies, we obtain $dN/dx$ from $dN/dx^*$ of Eq. (5):

$$\frac{dN}{dx}=\int_0^{\infty}aD\frac{(1-a'x)^d}{\sqrt{x^2+\left(\frac{2\mu}{\sqrt{s}}\right)^2}}g(p_T)dp_T \quad \left(D=\frac{d+1}{3},\ \ d=4.0\right). \tag{15}$$

Figure 5 shows the *x*-distributions, predicted by model 2, for various primary energies $E_0$. As can be seen in the figures, the Feynman scaling law is violated strongly both in the central region and in the forward region in model 2. There are almost no particles with $x\geqslant0.01$ at $E_0=10^{20}$ eV.

Figure 6 shows the energy dependence of charged multiplicity, predicted by the formulated models, after integration of Eq. (15). That is,

$$m(E_0)=\int\frac{dN}{dx}dx=\int_0^{1/a'}dx\int_0^{\infty}dp_T\frac{aD(1-a'x)^d}{\sqrt{x^2+(2\mu/\sqrt{s})^2}}g(p_T). \tag{16}$$

It is one of the merits of the present formulation that the *x* distribution is not divergent at $x=0$ owing to the term $2\mu/\sqrt{s}$. Recall that the lower limit of integration $m_\pi/E_0$ is introduced by hand in Eq. (4) to calculate the multiplicity. One can see in the figure that the difference in the multiplicity is small between model 1 and model 2 because we have

$$m(E_0)\simeq a\left[\ln\frac{\sqrt{s}}{\mu}-\ln a'\right].$$

That is, the parameter $a'$ appears in the form of $\ln a'$. It is no surprise that the energy dependence of model 2 agrees better with the experimental data than that of model 1.

Figure 6 shows also the energy dependence of the average total inelasticity in the laboratory system, defined by

$$\langle K\rangle\equiv\frac{3}{2}\int x\frac{dN}{dx}dx$$
$$=\frac{3}{2}\int_0^{1/a'}xdx\int_0^{\infty}dp_T\,aD\frac{(1-a'x)^d}{\sqrt{x^2+(2\mu/\sqrt{s})^2}}g(p_T). \tag{17}$$

It shows that the inelasticity decreases considerably in model 2 at high energies while it is constant (i.e., 0.5) in model 0 and in model 1.[8] It is worth noting that $\langle K\rangle=0.5$ holds when the relation $\alpha=\alpha'$ holds, irrespective of the values of $\alpha$ and $\alpha'$.

[7] The code does not necessarily predict the pseudo-rapidity density correctly in the forward region, because the observed pseudo-rapidity region by UA5 Collaboration is limited to $\eta^*\leqslant4.5$.

[8] It may look strange that the average inelasticity $\langle K\rangle$ is 0.5 for model 1, which has a higher rapidity density than QGSJET, since QGSJET found $\langle K\rangle\simeq0.6$. The effect is due to the difference in sampling of events, i.e., all inelastic events in the former and NSD events in the latter. In other words the average inelasticity by QGSJET is $\sim0.5$ for all inelastic events.

TABLE III. Dispersion of the pseudo-rapidity density distributions between model 2 and the simulation codes.

| Pseudo-rapidity range | UA5 code | SIBYLL | HDPM | QGSJET | VENUS | DPMJET |
|---|---|---|---|---|---|---|
| $\eta^* = 0.0 \sim 3.0$ ($x^* = 0 \sim 0.015$) | | | | | | |
| $S$ | 0.145 | 0.158 | 1.017 | 0.120 | 0.614 | 0.488 |
| $\sigma$ | 0.144 | 0.150 | 0.381 | 0.131 | 0.296 | 0.264 |
| $\eta^* = 3.5 \sim 6.0$ ($x^* = 0.024 \sim 0.3$) | | | | | | |
| $S$ | 0.198 | 0.563 | 0.563 | 1.054 | 2.974 | 2.974 |
| $\sigma$ | 0.182 | 0.306 | 0.306 | 0.419 | 0.704 | 0.704 |
| $\eta^* = 6.5 \sim 8.0$ ($x^* \geqslant 0.49$) | | | | | | |
| $S$ | 0.058 | 0.033 | 0.033 | 0.006 | 0.033 | 0.033 |
| $\sigma$ | 0.120 | 0.091 | 0.091 | 0.039 | 0.091 | 0.091 |

## III. SUMMARY

We have formulated the energy distribution of produced particles in multiple particle production, based on the direct observation data of cosmic-ray and accelerator experiments. The energy region covers $10^{12}$–$10^{14}$ eV.

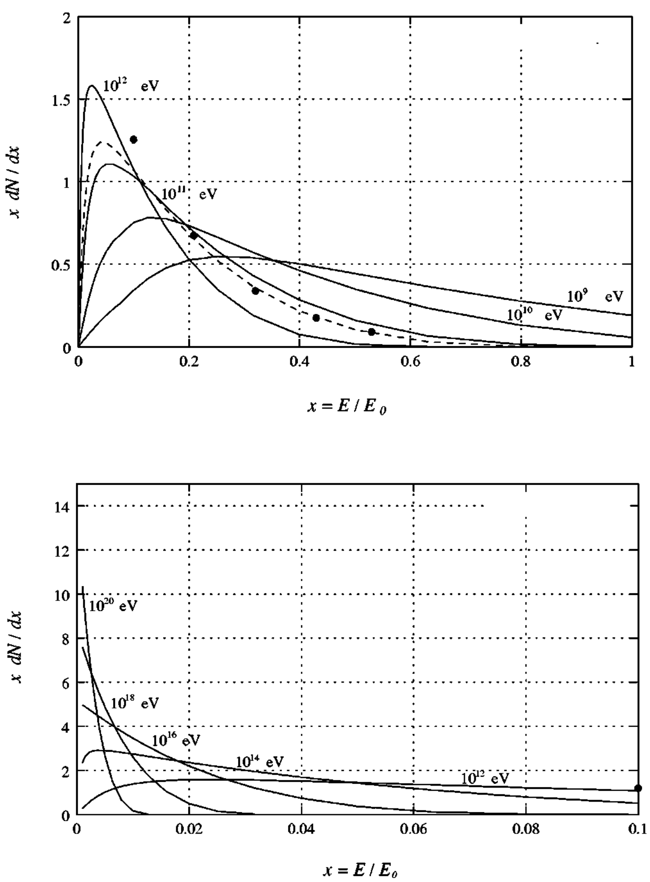


FIG. 5. $x$ distribution of model 2, $x(dN/dx)$, for various primary energies $E_0$. The chain line in the upper figure is the scaling function of Eq. (2) in the text. Full circles are experimental data of $p+p \rightarrow \pi^{ch}+X$ at $\sqrt{s}=20$ GeV [20], where the scaling law is valid. Model 2 shows the strong violation of Feynman scaling law both in the forward region and in the central region at high energies. The lower figure shows that the distribution in the forward region shrinks distinctly, in particular, at highest energies.

The formula shows clearly violation of the Feynman scaling law both in the central region and in the forward region. Hence we assume, following three models, that we need to extrapolate the energy distribution into a higher energy region (Table IV).

Average inelasticity is $\langle K \rangle = 0.5$ in model 0 and in model 1, but decreases with the incident energy in model 2. Most of the nuclear interaction models, which are employed in the simulations to follow the diffusion of cosmic rays in the atmosphere, lie between model 1 and model 2. The difference of the rapidity density distributions, predicted by respective models, is not negligibly small. This difference becomes probably larger at $\geqslant 10^{15}$ eV where the models are used to analyze high energy cosmic-ray data.

It was pointed out that the average inelasticity, which decreases with energy like that in model 2, is not compatible

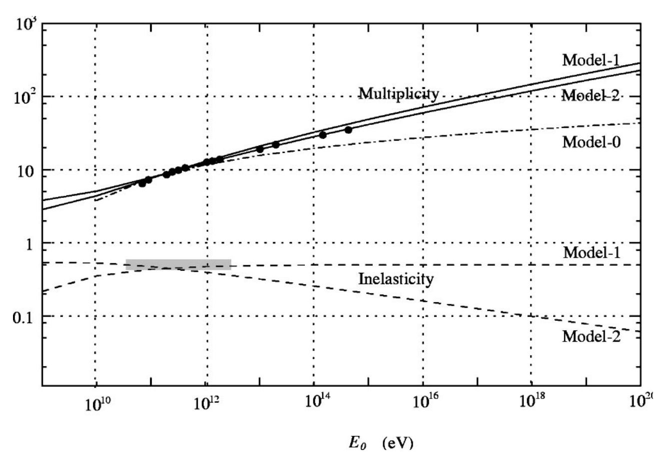


FIG. 6. Energy dependence of charged multiplicity and that of total inelasticity, predicted by the models. Experimental data of average charged multiplicity (full circles) is from bubble chambers, CERN Intersecting Storage Rings (ISR) and CERN Super Proton Synchrotron ($\mathrm{S}p\bar{p}\mathrm{S}$), compiled in Ref. [7]. The multiplicity is not different so much between model 1 and model 2. Model 2 describes the experimental data better than model 1, because model 2 has the best-fit parameters to describe the rapidity density distribution. Inelasticity is decreasing in model 2, while it is constant (=0.5) for model 0 and model 1. The shadowed area indicates the region where the Feynman scaling law, i.e., $\langle K \rangle = 0.5$, is verified by the experiments within the experimental errors.

TABLE IV. Formulated models in the present paper.

| | Feynman scaling law central region | Feynman scaling law forward region | Remark |
|---|---|---|---|
| Model 0 | valid | valid | Feynman scaling law, $\langle K\rangle=0.5$ |
| Model 1 | violated | violated | $\langle K\rangle=0.5$ |
| Model 2 | violated | violated | Best fit to the data |

with the altitude variation of the cosmic-ray intensities obtained by mountain emulsion chamber experiments [21]. We will examine in a following paper whether or not model 2, the best fit to the experimental direct observation data, describes the highest energy air showers at $\geqslant 10^{18}$ eV.

## ACKNOWLEDGMENTS

We are grateful for many discussions with the members of Chacaltaya Cosmic Ray Collaboration. The present study was made while one of the authors (E.H.S.) stayed in the Institute for Cosmic Ray Research, University of Tokyo. He is deeply indebted to all his friends at ICRR-UT for hospitality and support during his stay, while he was enjoying a sabbatical semester from his home institution.

## APPENDIX A: $p_T$-DISTRIBUTION

The parameter $p_0$ in Eq. (7) in the text is expressed by the rapidity $y^*$ in the following way:

$$p_0=\begin{cases} c & (y^*<y_0^*) \\ ce^{-c'(y^*-y_0^*)} & (y^*>y_0^*)\end{cases},$$

where $y_0^*$ corresponds to $x_0^*$. That is, by the definition of the rapidity we have

$$y_0^*\simeq \ln\left(\frac{\sqrt{s}}{\mu}x_0^*\right)=y_c+\ln\left(\frac{Mx_0^*}{\mu}\right).$$

The region $y^*>y_0^*$ is the forward region where $\langle p_T\rangle$ becomes smaller and $y_c=\ln(\sqrt{s}/M)$ ($M$: nucleon mass) is the rapidity of the incident nucleon.

According to the experimental data of the UA7 Collaboration [8],

$$y_0^*=y_c-1.5 \quad \text{and} \quad c'=\frac{1}{1.76}$$

at $\sqrt{s}=630$ GeV approximately. Therefore we have

$$\left\langle \ln\left(\frac{Mx_0^*}{\mu}\right)\right\rangle=-1.5 \qquad (\mu=\sqrt{p_T^2+m_\pi^2}),$$

which leads to $x_0^*=0.08$ because $\langle\ln(M/\mu)\rangle=1.0$.[9] The brackets $\langle\cdots\rangle$ mean the average with respect to the $p_T$-distribution $g(p_T)dp_T$.

Similarly we have, for the pseudo-rapidity $\eta^*$,

$$p_0=\begin{cases} c & (\eta^*<\eta_0^*) \\ ce^{-c'(\eta^*-\eta_0^*)} & (\eta^*>\eta_0^*)\end{cases}$$

with

$$\begin{aligned}\eta_0^* &= \ln\left(\frac{\sqrt{s}}{p_T}x_0^*\right)\\ &=y_c+\ln\left(\frac{Mx_0^*}{p_T}\right)\\ &=y_c+\ln\left(\frac{Mx_0^*}{\mu}\right)-\ln\left(\frac{p_T}{\mu}\right).\end{aligned}$$

It follows

$$\eta_0^*=y_c-1.3$$

because we have $\langle\ln(p_T/\mu)\rangle=-0.2$.

## APPENDIX B: $dN/dx$ AND $dN/dy$ OF $\gamma$ RAYS

The particle distribution of the Chacaltaya emulsion chamber experiment is expressed by the rapidity distribution of $\gamma$ rays which are the decay product of all $\pi^0$. Consequently we have to relate the distribution $dN/dx^*$ of charged pions in the text with that of $\gamma$-rays $dN_\gamma/dx_\gamma$. The derivation depends on smallness of $p_T/\sqrt{s}$ and $p_{T\gamma}/\sqrt{s}$ compared with $x^*$, because the experiment showed $\langle p_T\rangle\simeq 0.4$ (GeV/$c$), $\langle p_{T\gamma}\rangle\simeq 0.2$ (GeV/$c$), and $\langle\sqrt{s}\rangle=500$ GeV [6].

Guided by the distribution of pions $dN/dx$ in the text, we assume that the $x$ distribution of $\gamma$ rays is described by

$$\frac{dN_\gamma}{dx_\gamma dp_{T\gamma}}=\frac{h(x_\gamma)}{\sqrt{x_\gamma^2+(2p_{T\gamma}/\sqrt{s})^2}}g_\gamma(p_{T\gamma}),$$

[9] Then a small value of $x_0^*=0.08$ is not so surprising because $x^*=0.24$ at $y^*=y_c$. ($y_c$ is the rapidity of the incident nucleon which is considered the rapidity at the most forward region.) There are only 1.25 charged particles in the region $x^*>0.08$.

where the $g_\gamma(p_{T\gamma})dp_{T\gamma}$ is the $p_{T\gamma}$ distribution which will be given below. It has an approximate form of

$$\frac{dN_\gamma}{dx_\gamma} \simeq \frac{h(x)}{x_\gamma}$$

in the forward region where $x_\gamma \gg 2p_{T\gamma}/\sqrt{s}$.

We determine $h(x)$ by the fact that $\gamma$ rays are the decay product of all $\pi^0$. Due to the kinematics of $\pi^0 \to 2\gamma$ decay, we have

$$\begin{aligned}\frac{dN_\gamma}{dx_\gamma} &= \int_{x_\gamma}^{x_{max}} \frac{2}{x}\frac{dN_{\pi^0}}{dx}\\ &= \int_{x_\gamma}^{x_{max}} \frac{2}{x}\left(\frac{1}{2}\frac{dN}{dx}\right)\\ &= \int_{x_\gamma}^{x_{max}} \frac{1}{x}\int_0^\infty dp_T \frac{dN}{dx\,dp_T},\end{aligned}$$

where $dN/dx$ is the $x$ distribution of charged pions, given in the text. Since we are concerned with the distribution in the forward region of $x_\gamma \gg 2p_{T\gamma}/\sqrt{s}$, we have

$$\frac{dN_\gamma}{dx_\gamma} \simeq \int_{x_\gamma}^{x_{max}} \frac{Da(1-a'x)^d}{x^2}\int dp_T g(p_T),$$

where $x_{max}=1/a'$ and $\int g(p_T)dp_T=1$. Then we have

$$h(x)=Daa'\left[\frac{1}{a'}+4x\ln(a'x)+\frac{10}{3}x-6a'x^2+2a'^2x^3 -\frac{1}{3}a'^3x^4\right]$$

which has values $Da$ and 0 at $x=0$ and $x=1/a'$, respectively.

Therefore we have

$$\frac{dN_\gamma}{dy_\gamma dp_{T\gamma}} = h(x)g_\gamma(p_{T\gamma}) \qquad \left(x=\frac{p_{T\gamma}}{\sqrt{s}}(e^y-e^{-y})\right)$$

with

$$g_\gamma(p_{T\gamma})dp_{T\gamma}=\frac{p_{T\gamma}}{p_{0\gamma}^2}e^{-\frac{p_{T\gamma}}{p_{0\gamma}}}dp_{T\gamma}$$

where

$$p_{0\gamma}=\begin{cases} c_\gamma & (y_\gamma<y_{0\gamma})\\ c_\gamma e^{-c'_\gamma(y_\gamma-y_{0\gamma})} & (y_\gamma>y_{0\gamma})\end{cases} \qquad \left(c_\gamma=0.1\ \ \mathrm{GeV}/c, \quad c'_\gamma=\frac{1}{1.76}\right).$$


[1] Comparison between cosmic-ray data and nuclear interaction models is reviewed in A. Ohsawa, Nucl. Phys. B (Proc. Suppl.) **97**, 16 (2001).

[2] C. R. A. Augusto, S. L. C. Barroso, Y. Fujimoto, V. Kopenkin, M. Moriya, C. E. Navia, A. Ohsawa, E. H. Shibuya, and M. Tamada, Phys. Rev. D **61**, 012003 (2000).

[3] R. Feynman, Phys. Rev. Lett. **23**, 1415 (1969).

[4] F. E. Taylor, D. C. Carey, J. R. Johnson, R. Kummerud, D. J. Richie, A. Roberts, J. R. Sauer, R. Shafer, D. Theriot, and J. K. Walker, Phys. Rev. D **14**, 1217 (1976).

[5] T. K. Gaisser, R. J. Protheroe, K. E. Turver, and T. J. L. McComb, Rev. Mod. Phys. **50**, 859 (1978).

[6] J. A. Chinellato *et al.*, Suppl. Prog. Theor. Phys. **76**, 1 (1983).

[7] UA5 Collaboration, G. L. Alner *et al.*, Z. Phys. C **33**, 1 (1986); Nucl. Phys. **B291**, 445 (1987); Phys. Rep. **5**, 247 (1987).

[8] E. Pare, T. Doke, M. Haugenauer, V. Innocente, K. Kasahara, T. Kashiwagi, J. Kikuchi, S. Lazano, K. Masuda, H. Murakami, Y. Muraki, T. Nakada, A. Nakamoto, and T. Yuda, Phys. Lett. B **242**, 531 (1990).

[9] R. Haar, C. Liapis, P. Karchin, C. Biino, S. Erhan, W. Hofmann, P. Kreuzer, D. Lynn, M. Medinnis, S. Palestini, L. Pesando, M. Punturo, P. Schlein, B. Wilkens, and J. Zweizig, Phys. Lett. B **401**, 176 (1997).

[10] C. M. G. Lattes *et al.*, Suppl. Prog. Theor. Phys. **47**, 1 (1971).

[11] A. Ohsawa, Prog. Theor. Phys. **92**, 1005 (1994).

[12] CDF Collaboration, F. Abe *et al.*, Phys. Rev. D **41**, 2330 (1990).

[13] J. Knapp, D. Heck, and G. Schatz, Forchungszentrum Karlsruhe, FZKA 5828, 1996 (to be published).

[14] UA5 Collaboration, G. J. Alner *et al.*, CERN-EP/86-213.

[15] K. Werner, Phys. Rep. **232**, 87 (1993).

[16] N. N. Kalmykov and S. S. Ostapchenko, Yad. Fiz. **56**, 105 (1993) [Phys. At. Nucl. **56**, 346 (1993)]; N. N. Kalmykov, S. S. Ostapchenko, and A. I. Pavlov, Bull. Acad. Sci. USSR, Phys. Ser. (Engl. Transl.) **58**, 1966 (1994).

[17] R. S. Fletcher, T. K. Gaisser, P. Lipari, and T. Stanev, Phys. Rev. D **50**, 5710 (1994); J. Engler, T. K. Gaisser, P. Lipari, and T. Stanev, *ibid.* **46**, 5013 (1992).

[18] J. N. Capdevielle *et al.*, Kernforschungszentrum Karlsruhe KfK Report No. 4998, 1992.

[19] J. Ranft, Phys. Rev. D **51**, 64 (1995).

[20] M. Adams *et al.*, Z. Phys. C **39**, 257 (1988).

[21] A. Ohsawa and K. Sawayanagi, Phys. Rev. D **45**, 3128 (1992).